The effect of cardiac output on the pharmacokinetics and pharmacodynamics of propofol during closed-loop induction of anesthesia

A. Savoca [a], K. van Heusden [b], D. Manca [a,*], J.M. Ansermino [c], G.A. Dumont [b,c]

[a] PSE-Lab, Process Systems Engineering Laboratory, Dipartimento di Chimica, Materiali e Ingegneria Chimica "Giulio Natta", Politecnico di Milano, Piazza Leonardo da Vinci 32, Milano 20133, Italy
[b] Department of Electrical & Computer Engineering, The University of British Columbia, Vancouver, British Columbia, Canada
[c] Department of Anesthesiology, Pharmacology & Therapeutics, The University of British Columbia, Vancouver, British Columbia, Canada

ARTICLE INFO

Article history:
Received 26 November 2019
Revised 31 January 2020
Accepted 17 February 2020

Keywords:
Cardiac output
Hemodynamics
Closed-loop anesthesia
Physiologically-based pharmacokinetic modeling
Propofol
High-risk patients

ABSTRACT

Background and objective: Intraoperative hemodynamic stability is essential to safety and post-operative well-being of patients and should be optimized in closed-loop control of anesthesia. Cardiovascular changes inducing variations in pharmacokinetics may require dose modification. Rigorous investigational tools can strengthen current knowledge of the anesthesiologists and support clinical practice. We quantify the cardiovascular response of high-risk patients to closed-loop anesthesia and propose a new application of physiologically-based pharmacokinetic-pharmacodynamic (PBPK-PD) simulations to examine the effect of hemodynamic changes on the depth of hypnosis (DoH).

Methods: We evaluate clinical hemodynamic changes in response to anesthesia induction in high-risk patients from a study on closed-loop anesthesia. We develop and validate a PBPK-PD model to simulate the effect of changes in cardiac output (CO) on plasma levels and DoH. The wavelet-based anesthetic value for central nervous system monitoring index (WAV_{CNS}) is used as clinical end-point of propofol hypnotic effect.

Results: The median (interquartile range, IQR) changes in CO and arterial pressure (AP), 3 min after induction of anesthesia, are 22.43 (14.82-36.0) % and 26.60 (22.39-35.33) % respectively. The decrease in heart rate (HR) is less marked, *i.e.* 8.82 (4.94-12.68) %. The cardiovascular response is comparable or less enhanced than in manual propofol induction studies. PBPK simulations show that the marked decrease in CO coincides with high predicted plasma levels and deep levels of hypnosis, *i.e.* $WAV_{CNS} < 40$. PD model identification is improved using the PBPK model rather than a standard three-compartment PK model. PD simulations reveal that a 30% drop in CO can cause a 30% change in WAV_{CNS}.

Conclusions: Significant CO drops produce increased predicted plasma concentrations corresponding to deeper anesthesia, which is potentially dangerous for elderly patients. PBPK-PD model simulations allow studying and quantifying these effects to improve clinical practice.

1. Introduction

Propofol is an intravenous (IV) hypnotic agent commonly used for induction of general anesthesia. Along with the advantages of rapid onset of unconsciousness and short duration of action, propofol has adverse effects such as cardiorespiratory depression and hypotension. These adverse effects are characterized by slower dynamics compared to the hypnotic effects [1].

Hypotension following anesthetic drug administration in the operating room is common, including hypotension sufficiently severe to require an intervention such as vasoconstrictive drug administration to counter the hemodynamic response. Cardiovascular changes following propofol administration show high inter-individual variability and are associated with the patients' characteristics. Age over 50 year, pre-induction mean arterial pressure (MAP) values below 70 mmHg, and American Society of

* Corresponding author.
E-mail address: davide.manca@polimi.it (D. Manca).

https://doi.org/10.1016/j.cmpb.2020.105406

Anesthesiologists (ASA) classification III and IV are reported predictors of hemodynamic fluctuations [2]. Although mild hypotension is considered clinically insignificant [2], association of intraoperative hemodynamic instability with mortality, stroke, and other adverse outcomes has been shown [2, 3]. Currently, there is lack of evidence that commonly used target-controlled infusion (TCI) systems reduce the chances of hemodynamic fluctuations, compared to manual induction [4]. One of the goals of adoption of automated control systems in anesthesia is to increase the stability of the patients' anesthetic state, including their hemodynamics.

Induction of anesthesia is a challenging phase from the point of view of the hemodynamic response. Heart-rate (HR) and (non-invasive) blood pressure (BP) are routinely measured in clinical practice, during both induction and maintenance of anesthesia. Cardiac output (CO) monitoring on the other hand, is not as commonly used, and is generally employed at the discretion of the anesthetist in high-risk patients and/or major surgical procedures [5]. Reports of CO changes following propofol induction of anesthesia often feature few observations [6, 7], with limited frequency [8, 9], or over a short time horizon [10, 11]. Evaluation and design of closed-loop controllers often focus on depth-of-hypnosis (DoH) rather than the hemodynamic aspects (*e.g.*, [12-14]).

Hemodynamic changes are also reported to affect the pharmacokinetics of anesthetic and analgesic drugs [15-17] with consequent variations in dosing requirements. CO is reported to be a key determinant of propofol pharmacokinetics [15, 18]. In particular, pharmacokinetic studies in animals show that lower cardiac outputs lead to higher plasma concentrations [15, 18]. This is in line with the clinical experience according to which reduced CO leads to lower anesthetic requirements (also evident in the case of critical events, such as hemorrhage [17]). Thus, neglecting the effect played by CO can lead to potential overdosing of propofol, which can be dangerous, especially for critically ill and/or elderly patients.

Physiologically-based pharmacokinetic (PBPK) models can account for the effect of CO changes [19]. The PBPK modeling approach is based on a simplified but nonetheless physiological description of the drug distribution and transport in the body organs and tissues, which are assimilated to homogenous compartments. Thus, the effect of CO on blood flowrates can be accounted for and the effect of CO changes on the pharmacokinetics can be studied *in silico*. When combined with a suitable pharmacodynamic (PD) model, the implications on the depth of hypnosis can also be investigated *in silico*.

The objectives of this paper are (i) to quantify CO, MAP, and HR changes observed during closed-loop induction of propofol-remifentanil anesthesia, for a high-risk subset of the population for whom arterial blood pressure monitoring was indicated in [20], and (ii) to investigate the influence of CO changes on pharmacokinetics and pharmacodynamics via *in silico* simulations based on PBPK-PD modelling.

2. Methods

2.1. Clinical data

Data were available from the clinical evaluation of closed-loop control of propofol-remifentanil anesthesia, based on the wavelet-based anesthetic value for central nervous system monitoring index (WAV_{CNS}) index provided by the NeuroSENSE NS-701 monitor (NeuroWave Systems, Cleveland Heights, OH) [20]. Ethical approval from the Research Ethics Board (FHREB 2012-056), investigational device approval from Health Canada (206188), and patients' informed consent were previously obtained [20]. In a subset of 15 patients, an arterial line was placed prior to induction of anesthesia, and continuous CO measurements during induction of anesthesia were available (LiDCO Rapid, LiDCO Ltd, London UK). HR was recorded using ECG (Carescape B850 multi-parameter monitor, GE Healthcare, Buckinghamshire, UK). This subset of the study population represents an "at-risk" population because of their conditions or type of surgery, for whom arterial line placement was indicated. Table 1 reports the demographics of the studied subset. Data on CO, BP, and HR were analyzed using MATLAB (MathWorks, Natick, MA).

Table 1
Demographics of the 15 patients' cohort. Age and BMI are presented as median (interquartile range, IQR).

N	15
Gender (F:M)	1:14
Age (y)	67 (59-73)
BMI (kg/m^2)	28.22 (25.49-30.34)

2.2. Propofol physiologically-based pharmacokinetic model

In silico investigation of the effect of CO changes on pharmacokinetics is performed using a PBPK model that was developed and validated using data available in the literature, and has been applied to *in silico* simulation of closed-loop controlled anesthesia [21]. The structure of this model is adapted from the more complex PBPK model described in [22] to meet propofol pharmacokinetic characteristics. The absorption, distribution, metabolism, and excretion (ADME) processes undergone by propofol within the body are described via material balances over five compartments, corresponding to specific tissues and organs.

The number of compartments is a compromise between the mathematical complexity (along with consequent identifiability controversies) and the anatomical and physiological resemblance of the model. The following compartments are included: plasma (P), gastrointestinal circulatory system (GICS), liver (L), highly perfused organs (HO, which lump the kidneys, brain, spleen, and heart), and poorly perfused tissues (PT, which lump fat, muscles, bones, and skin). For the sake of clarity, GICS comprises the portal vein, the mesenteric artery, and the microvessels that are involved in the blood transport to and from the gastrointestinal system. The plasma compartment balance Eq. (1)) features the input infusion rate, IR(t), as administered by the controller in [20]. The mathematical formulation of the model consists of Eqs. (1)-((5) that describe the dynamics of propofol concentration C(t) in the body compartments, complemented by Eqs. 6) and ((7), whose purpose is to describe and quantify the eliminated drug amount via the hepatic (H) and extra-hepatic (EH) routes (for propofol case, renal and tissues pathways).

As opposed to classical three-compartment PK models, not all the parameters of the PBPK model are identified with PK data (*i.e.* measured values of blood concentration) of a specific population. There are three categories of parameters: (i) individualized, *i.e.* calculated from the demographics, (ii) assigned, *i.e.* specific values related to the drug physiochemical characteristics that are available in the literature, and (iii) regressed with PK data. Table 2 lists the model parameters and clarifies the method for their identification.

The calculation of compartment volumes V^i depends on the demographics (specifically, correlations account for patients' body surface area, height, age, and gender [23]) and allows for individualization of the pharmacokinetic prediction. The protein binding fraction, R, is assigned according to the scientific literature on propofol [24]. In Eqs. (1-5), Q^{HV},Q^{PV}, and Q^{HA} are the blood flows respectively through the hepatic vein (HV), the portal vein (PV), and the hepatic artery (HA), which are calculated as a fraction of the CO. The same approach is applied to renal clearance CL^K calculated from the total blood flowrate to kidneys, Q^K, which is evalu-

Table 2
List of PBPK model parameters, symbols, and calculation method[1].

Parameter	Symbol	Identification
Organ/tissue density	ρ_i	Assigned as in [30]
Blood weight	W^B	Calculated from demographics (as in [23])
PT weight	W^{PT}	Calculated from demographics (as in [23])
HO weight	W^{HO}	Calculated from demographics (as in [23])
Liver weight	W^L	Calculated from demographics (as in [23])
Blood volume	V^B	Calculated as W^B/ρ_B
Hematocrit	h	Assigned as in [23]
Plasma volume	V^P	Calculated as $V^B(1-h)$
PT volume	V^{PT}	Calculated as W^{PT}/ρ_{PT}
HO volume	V^{HO}	Calculated as W^{HO}/ρ_{HO}
GICS volume	V^{GICS}	Calculated as in [22]
Liver volume	V^L	Calculated as W^L/ρ_L
HV blood flow	Q^{HV}	Calculated as %CO (as in [23])
HA blood flow	Q^{HA}	Calculated as $25\%Q^{HV}$
PV blood flow	Q^{PV}	Calculated as $75\%Q^{HV}$
Kidneys blood flow	Q^K	Calculated as %CO (as in [23])
Hepatic clearance	CL^H	Calculated as $Eff^H Q^{PV}$
Renal clearance	CL^K	Calculated as $Eff^K Q^K$
Protein binding fraction	R	Assigned as in [24]
PT-plasma transport coefficient	k_{PT-P}	Identified with data from Schnider et al. [25]
Plasma-PT transport coefficient	k_{P-PT}	Identified with data from Schnider et al. [25]
HO-plasma transport coefficient	k_{HO-P}	Identified with data from Schnider et al. [25]
Plasma-HO transport coefficient	k_{P-HO}	Identified with data from Schnider et al. [25]
GI tissue metabolic constant	$k_{EL,GI}$	Identified with data from Schnider et al. [25]
Hepatic efficiency	Eff^H	Identified with data from Schnider et al. [25]
Renal efficiency	Eff^K	Identified with data from Schnider et al. [25]

ated as a fraction of CO (see Table 2). Correlations for calculation of blood flowrates depend on body surface area, height, age, gender [23].

$$\frac{dC^P(t)}{dt} = \frac{IR(t)}{V^P} + C^{PT}(t)k_{PT-P}\frac{V^{PT}}{V^P} + C^L(t)\frac{Q^{HV}}{V^P} + C^{HO}(t)k_{HO-P}\frac{V^{HO}}{V^P} - \frac{C^P(t)}{V^P}CL^K - C^P(t)\left(k_{P-PT}(1-R) + k_{P-HO}(1-R) + \frac{Q^{HA}}{V^P} + \frac{Q^{PV}}{V^P}\right) \quad (1)$$

$$\frac{dC^{GICS}(t)}{dt} = -C^{GICS}(t)\frac{Q^{PV}}{V^{GICS}} + C^P(t)\frac{Q^{PV}}{V^{GICS}} - C^{GICS}(t)k_{EL,GI} \quad (2)$$

$$\frac{dC^L(t)}{dt} = -C^L(t)\left(\frac{Q^{HV}}{V^L} + \frac{CL^H}{V^L}\right) + C^P(t)\frac{Q^{HA}}{V^L} + C^{GICS}(t)\frac{Q^{PV}}{V^L} \quad (3)$$

$$\frac{dC^{HO}(t)}{dt} = -C^{HO}(t)k_{HO-P} + C^P(t)k_{P-HO}(1-R)\frac{V^P}{V^{HO}} \quad (4)$$

$$\frac{dC^{PT}(t)}{dt} = -C^{PT}(t)k_{PT-P} + C^P(t)k_{P-PT}(1-R)\frac{V^P}{V^{PT}} \quad (5)$$

$$\frac{dA^{EL,L}(t)}{dt} = C^L(t)CL^H \quad (6)$$

$$\frac{dA^{EL,K}(t)}{dt} = C^P(t)CL^K + V^{GICS}C^{GICS}(t)k_{EL,GI} \quad (7)$$

The remaining parameters (*i.e.* transport coefficients, *e.g.*, k_{P-PT} and metabolic constants, *e.g.*, Eff^H) are identified via nonlinear regression with pharmacokinetic data from Schnider et al. [25]. The model, with CO calculated from the demographics (as in [23]) was validated using PK data from four studies in different populations [26-29].

Table 3 reports the validation results in terms of median prediction error (MDPE) and median absolute prediction error (MDAPE). MDPE and MDAPE are chosen as predictive performance indicators because they are commonly used in the scientific literature related to pharmacokinetic modeling of IV drugs employed in anesthesia and analgesia. Acceptable values are MDPE in the range within ±20% and MDAPE 20–40% (mean values) [31, 32]. Although some values are outside these target ranges, the variability of patients' characteristics in the validation studies (*i.e.* young, elderly, healthy, critically ills, and obese) and infusion regimes (boluses and infusions) must be taken into account. Indeed, in case of critically ill patients [28, 29], concomitant drugs and comorbidities may influence propofol pharmacokinetics, with repercussions on the poorer predictive performance of the model. The Dyck and Shafer dataset [27] features a peculiar characteristic compared to other propofol pharmacokinetic datasets, as most blood samples were obtained up to 19 h after a 10-min IV propofol infusion. This means that most values refer to propofol sub-anesthetic concentrations. Likely, the model prediction would be superior if propofol concentrations were evaluated only during the maintenance and early elimination phases of the infusion, as in other propofol pharmacokinetic datasets. Future work should address the issue of further adapting the correlations used to identify the model parameters (see Table 2) to obese patients, as their condition involves anatomical and physiological changes that, depending on the degree of obesity, will alter propofol pharmacokinetics compared to healthy individuals. By doing so, the model prediction of Servin's dataset [26] would be improved.

The effect of CO on pharmacokinetics is evaluated using propofol infusion rates as well as the measured CO data [20] as inputs to the PBPK model to simulate the pharmacokinetics of the patients. Hence, CO changes will affect the drug transport and final concentration within the body. Resulting PK profiles are compared to the Schnider-model predicted levels [25].

2.3. *Pharmacodynamic modeling and* in silico *evaluation*

The phase-lag between the time course of the plasma concentration and manifestation of the pharmacological effect is accounted for by the commonly-used effect-site equation approach. The PBPK model is combined with a suitable form of the Hill equation, whose PD parameters are identified via nonlinear regression

Table 3
Validation results of the PBPK model. First column reports the PK study (number and type of subjects involved), second and third columns list MDPE and MDAPE (mean (SD))[2].

PK study	MDPE%	MDAPE%
Servin et al. [26] ($N = 8$, obese)	4.05 (27.1)	40.2 (28.2)
Gepts et al. [29] ($N = 16$, critically ill)	−26.22 (36.96)	51.06 (31.77)
Dyck & Shafer [27] ($N = 57$, healthy)	−14.8 (21.2)	40.6 (16.3)
Smuszkiewicz et al. [28] ($N = 1$, critically ill)	−29	29

Table 4
Median (IQR) values of CO, MAP, and HR drop 1.5 and 3 min after the start of induction. Median (IQR) values of the maximum drop are also reported ($N = 15$)[3].

	%ΔCO [-]	%ΔMAP [-]	%ΔHR [-]
1.5 min	7.03 (1.66-17.47)	8.93 (3.11-16.1)	5.45 (2.48-9.13)
3 min	22.43 (14.82-36.0)	26.6 (22.39-35.33)	8.82 (4.94-12.68)
max	43.43 (38.57-47.74)	37.5 (32.79-52.25)	16.28 (12.99-20.36)

using the WAV_{CNS} data from West et al. [20]. The goodness-of-fit is evaluated via Root-Mean-Square Error (RMSE) for the PBPK-PD and Schnider three-compartment PK-PD models of the 15 patients.

The effect of different extents of CO decrease on pharmacodynamics is evaluated for a virtual patient described by a validated PBPK-PD model. The DoH is predicted for three different CO profiles, representing a 35, 50, and 70% (maximum) drop.

3. Hemodynamic changes during closed-loop induction of anesthesia

Section 3.1 presents the hemodynamic changes observed during induction of anesthesia in the high-risk subset of the patient population in [20]. Section 3.2 discusses these results and compares them to reported changes following manual induction of anesthesia with propofol in similar patients.

3.1. Quantification of hemodynamic changes

Baseline values for the 15 patients in the subpopulation are median (IQR) CO 7.24 (5.57-8.02) L/min, MAP 106.6 (95-111.25) mmHg and HR 71 (58.75-78.25) b/min. 27% of the patients exhibited baseline values of CO and HR lower than 5 L/min and 60 b/min, respectively, which is not atypical considering age and ASA classes (II-III). Induction of anesthesia was performed in closed-loop. The end of induction of anesthesia was defined as the time the $WAV_{CNS} < 60$ for 30 consecutive seconds. For the 15 patients in the subpopulation, this was achieved in a median (IQR) 4.18 min (3.44-4.54 min) with a propofol dose of 1.42 (1.05-1.47) mg/kg.

Table 4 reports median (IQR) values of the drops in CO, MAP, and HR 1.5 and 3 min after induction of anesthesia. Whereas the drop in CO and MAP after 3 min is median 22.4 and 26.6%, respectively, the decrease in HR is less marked. The maximum values of the drop (*i.e.* evaluated between the start of induction and the start of the airway management) are 43.43% and 37.5% for CO and MAP, respectively (also reported in Table 4). Note that median maximum MAP drop exceeds 30%, which is typically considered clinically significant.

In some of the patients, the CO continued to decrease further after 3 min, in particular to over 50% for 1 patient and over 60% for 2 patients. However, although in some of these cases this enhanced reduction may have been caused by propofol overdosing, other factors may have contributed.

Fig. 1 shows the individual trends of CO, MAP, and HR (top panel) from the start of induction until induction is completed, as defined above. The bottom panel shows median (IQR) values over the first 5 min after the start of propofol induction. The individual trends of CO, MAP, and HR drop (Fig. 1) and IQR associated to the drop (Table 4) manifest great inter-individual variability. Variability of the profiles may be partly ascribed to the differences in the patients' characteristics, diseases and physical conditions, timing of intubation, type of surgical procedure, and drug-drug interactions.

3.2. Hemodynamic changes after manual induction in the literature and discussion

In 15 high-risk patients scheduled for cardiac surgery, Singh et al. [33] administered propofol 1.5 mg/kg and fentanyl 4 µg/kg. They recorded baseline and 1-min interval values of the hemodynamic variables for 3 min after induction of anesthesia. HR and MAP were recorded continuously, and CO was measured with the FloTrac-Vigileo monitor (Edwards Life Sciences, Irvine, USA), based on the analysis of the arterial pressure waveform. They found 18.7 and 17.3% decrease in CO and MAP and no statistically significant change in HR after 1 min, and mean 37.5, 34.3, and 10.5% decrease in CO, MAP, and HR after 3 min from induction.

Hemodynamic variables were continuously monitored in [34] with the Nexfin monitor (Edwards LifeSciences Corporation, Irvine, CA, USA), a non-invasive pulse pressure analysis device, in 40 patients (ASA I-II-III) administered with propofol (1-3 mg/kg) and remifentanil (1 µg/kg). A decrease of mean 30, 23.8, and 26% was found in CO, MAP, and HR after induction.

In [8], CO, MAP, and HR were recorded continuously (CO was measured using the LiDCO Plus system (LiDCO, London, UK)) during manual induction of anesthesia with 1.5-2.5 mg/kg of propofol and 0.5 µg/kg of remifentanil in 24 patients (ASA II-III). Baseline values as well as the value of CO, MAP, and HR after induction (defined as 3 min after BIS < 60) and after intubation are given. They observed about 29% decrease in CO, and 22% in MAP and HR (mean values). It was noted that the open lung surgery may have contributed to the circulatory instability due to tissue hypoperfusion and thus affected these results [8].

In 10 elderly patients (ASA I-II) scheduled for abdominal surgery, anesthesia was induced with 1.5 mg/kg of propofol [6]. A catheter in the radial artery was inserted for continuous monitoring of arterial blood pressure, and cardiac output was measured by the thermodilution technique. Lowest values after induction were reported. There was no statistically significant change in HR, whereas a decrease of 17.5 and 33.3% in CO and MAP (mean values) was observed.

Reported HR changes are contradictory. HR is more affected by external stimuli, and differences in the study design (*e.g.*, times to intubation and to measurement of baseline values) and patients' level of anxiety are likely to produce inconsistencies. Although, lowest values were not reported (except for one study) the median changes in CO and MAP observed after 1.5 and 3 min in this subpopulation of the closed-loop study in [20] are comparable or smaller than the changes described in the literature following manual induction of anesthesia with propofol. Thus, closed-loop induction did not introduce a higher risk of hypotension and cardiovascular changes compared to manual induction. In fact, de-

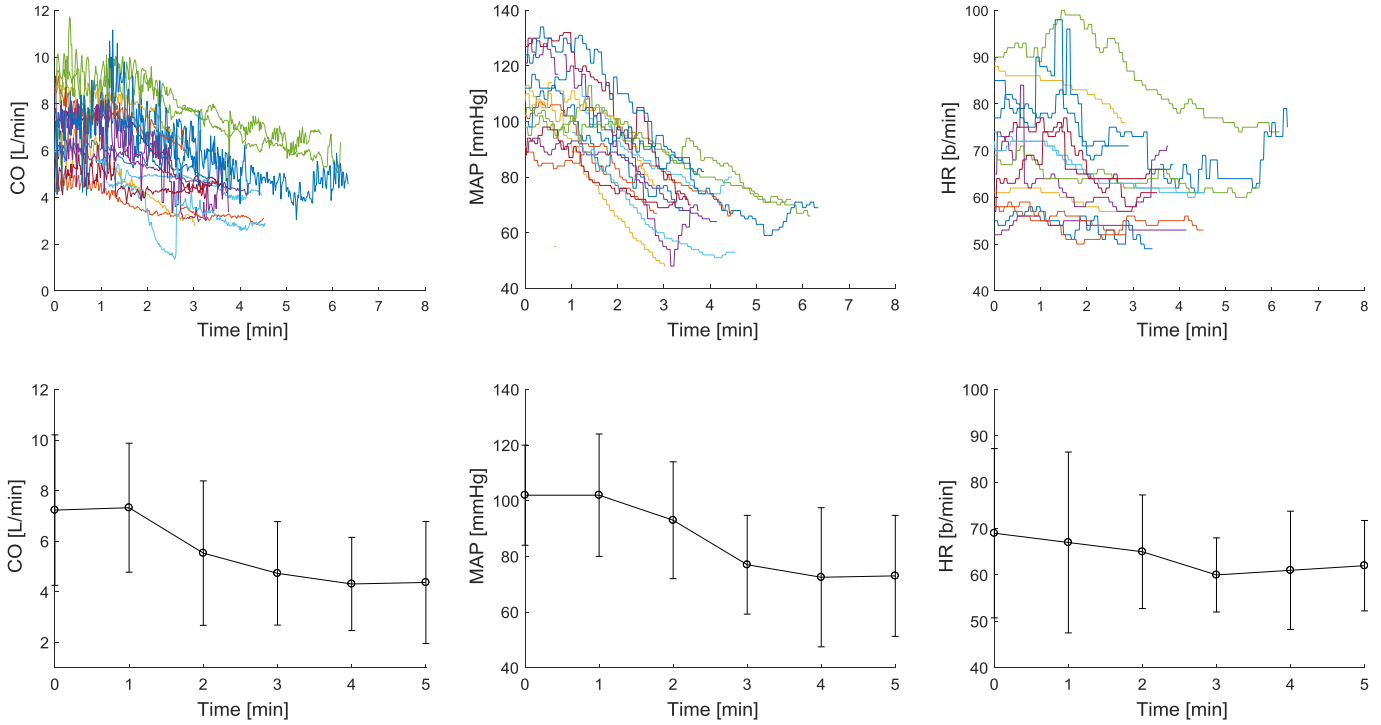

Fig. 1. (Top panel) Individual patients' trends of CO, MAP, and HR throughout the induction period (*i.e.* from the start of induction to completed induction). (Bottom panel) Median (IQR) values of CO, MAP, and HR in the first 5 min after the start of propofol induction.

spite the age and condition of the patients, and the procedures in this subpopulation where use of an arterial line was selected, the control action provides an overall adequate compromise between hemodynamic stability and velocity of induction. Note that patients' characteristics, technology used to measure CO, drug dosing, and opioid use differ among studies, and need to be taken into account in the interpretation of this comparison.

4. Impact on pharmacokinetics and pharmacodynamics

This section presents the results of *in silico* evaluation of the effect of CO on pharmacokinetics and pharmacodynamics. The resulting pharmacokinetic profiles of the PBPK simulations and the commonly used three-compartment Schnider model [25] are compared in Section 4.1 for six representative cases.

Section 4.2 presents the results of identification of PD models for DoH using the PBPK and the Schnider PK models. *In silico* simulations of one of the PBPK-PD models are presented to evaluate the effect of different CO changes on the DoH in Section 4.3.

4.1. PBPK prediction of plasma levels

Plasma concentrations are predicted for the 15 patients described in Section 2.1, using the PBPK model presented in Section 2.2. Input to the model are demographics of those patients, infusion rate as administered by the controller, and the measured CO.

Figs. 2 and 3 show the measured CO (A Panels), the simulated dynamics of propofol concentration (B Panels), and the measured DoH (C Panels) of six representative cases, referred to as cases 1, 2, and 3 (in Fig. 2), and cases 4, 5, and 6 (in Fig. 3).

The considered time horizon is 15 min after the start of induction of anesthesia. Missing data in the CO trends are due to either monitors disconnection or artifacts that were suitably removed in the data post-processing phase.

The PBPK-predicted plasma concentrations (red dashed line) exceed the plasma concentrations predicted by the Schnider model (blue continuous line). Discrepancies in the plasma levels prediction resulting from different PK models, are not surprising, and have been reported extensively [35, 36]. It is known that early disposition propofol is not well-characterized by classical three-compartment models [37]. Concentration peaks in the range between 20-30 µg/mL have been found after bolus administration [38]. Higher concentrations have been found in the elderly compared to younger patients [39]. Although the Schnider model features age as covariate, studies in the elderly have shown underestimation of the Schnider PK-prediction with respect to the measured values (see positive MDPEs reported by Vuyk et al. [40] and Cortinez et al. [41]). Considering the patient population and the corresponding DoH overshoot and cardiovascular depression, PBPK-predicted levels are realistic.

Note that the PBPK-predicted plasma concentration shows close resemblance to the WAV_{CNS} data trend (see for instance the plasma peak (red dashed line) and the DoH drop below 40 in cases 2 and 3). In fact, cases 1, 2, and 3 (Fig. 2) manifest DoH values that are below the recommended lower level of 40 for short periods, and display burst suppression behavior.

This behavior corresponds, with some delay, to high peaks (>10 μg/mL) in the concentration trend as a result of the changes in CO. Instead, in cases 4, 5, and 6 (Fig. 3), the CO drop is more gradual and limited ($\%\Delta CO_{max} < 45$) and the DoH trend does not indicate an overshoot and values < 40. Corresponding predicted peak plasma levels are approximately 10 μg/mL. These results confirm that the hypnotic effects of propofol infusion may be amplified by significant CO decreases, in line with the experience from the clinical practice that adjusts drug dosing in case of patients with low CO baseline. On the other hand, PK prediction according to Schnider model prediction does not manifest abnormal levels: in fact, levels represented by the blue continuous line are comparable in most cases, except case 2.

The fact that deep levels of hypnosis are found in conjunction with higher predicted plasma levels, (Fig. 2), may also suggest that significant changes in CO are a contributing factor to the dynamics

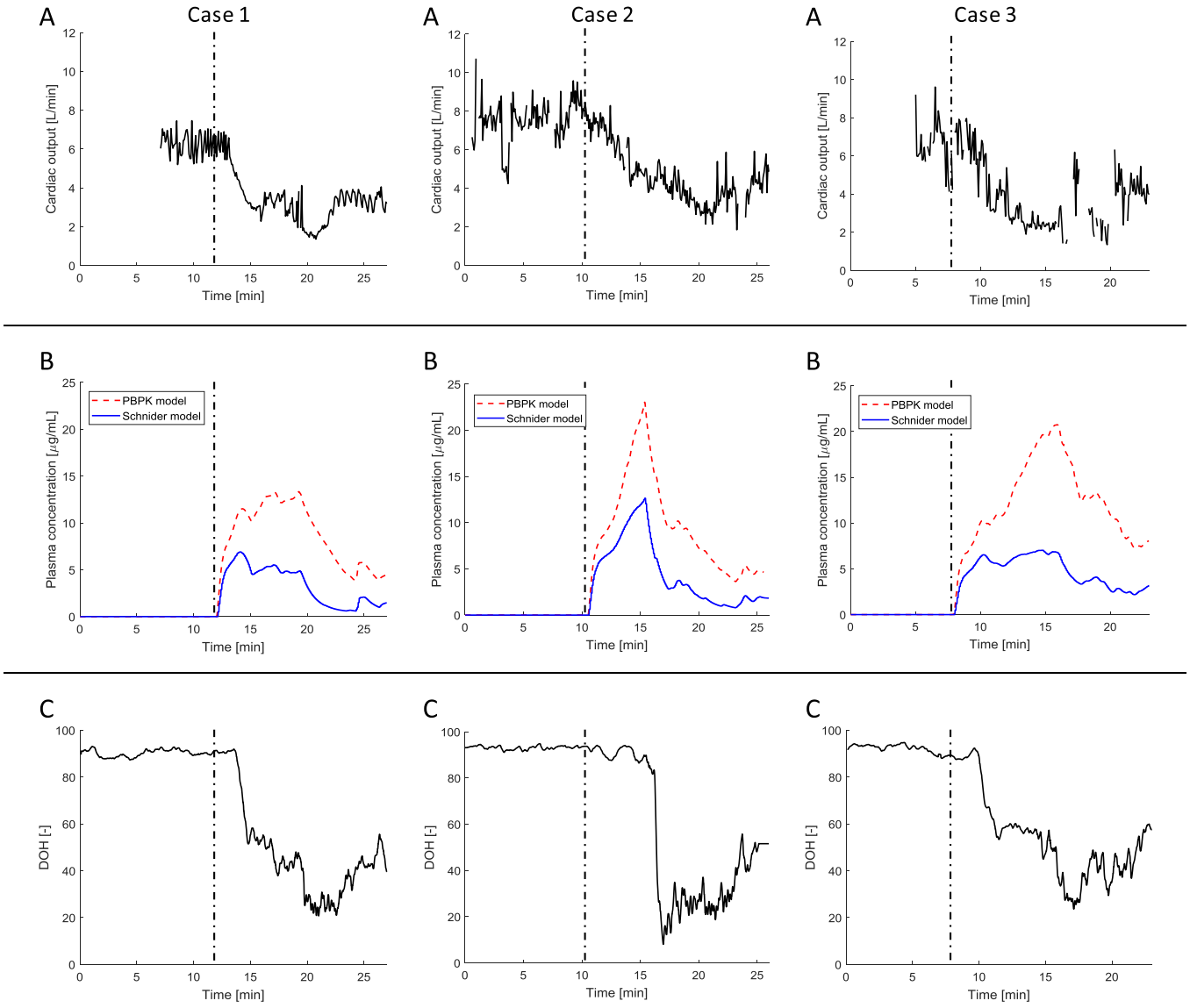

Fig. 2. Panel A shows the CO trends of the individual patients (cases 1, 2, and 3). Panel B shows the comparison between the plasma concentration dynamics predicted by our PBPK model (red dashed line) and Schnider model (blue continuous line). Panel C shows corresponding trends of the WAV_{CNS} index as DoH measure. The black dashed-dotted vertical line marks the start of propofol infusion. (For interpretation of the references to color in this figure legend, the reader is referred to the web version of this article.)

of propofol concentration in the brain with consequence of burst suppression.

In addition, these trends are often observed in presence of MAP (not shown) equal to or below 70 mmHg, which is the reference lower bound for preservation of cerebral blood flow autoregulation [42]. Actually, low DoH values have been reported in association with both overdosing and reduced cerebral perfusion [43], hence in this case there may be a concomitant effect of overdosing and low cerebral perfusion resulting in burst suppression.

4.2. PD model identification

DoH data from West et al. [20] were used to identify PD models of the 15 patients via nonlinear regression. Table 5 shows RMSE values for the PBPK-PD and the three-compartment PK-PD models. A lower value of RMSE is obtained in the cases of PBPK-PD models identified particularly with DoH data of patients subject to marked CO decreases ($\%\Delta CO_{max} > 45$).

Table 5
RMSE values (median (IQR)) for the PBPK-PD and Schnider PK-PD models.

Patients	PBPK-PD RMSE	Schnider PK-PD RMSE
All ($N = 15$)	5.72 (4.67-5.99)	5.90 (5.07-6.84)
$\%\Delta CO_{max} > 45$ ($N = 6$)	5.60 (5.34-5.85)	6.26 (5.54-7.2)

The differences in the concentration trends discussed in Section 4.1 allow for improving the fit, because DoH is modeled via a modified Hill equation, as a function of propofol effect-site concentration [21]. Since the three-compartment PK model predicts less marked plasma concentration peaks, the slower effect-site concentration dynamics cannot describe significant DoH drops and overshoot (mostly evident in the six cases where $\%\Delta CO_{max} > 45$, see improved RMSE shown in Table 5). As a representative case, Fig. 4 shows the identified PBPK-PD and three-compartment PK-PD models of case 1, which is also used in Section 4.3 to simulate *in silico* the effect of CO on pharmacodynamics. Right panel

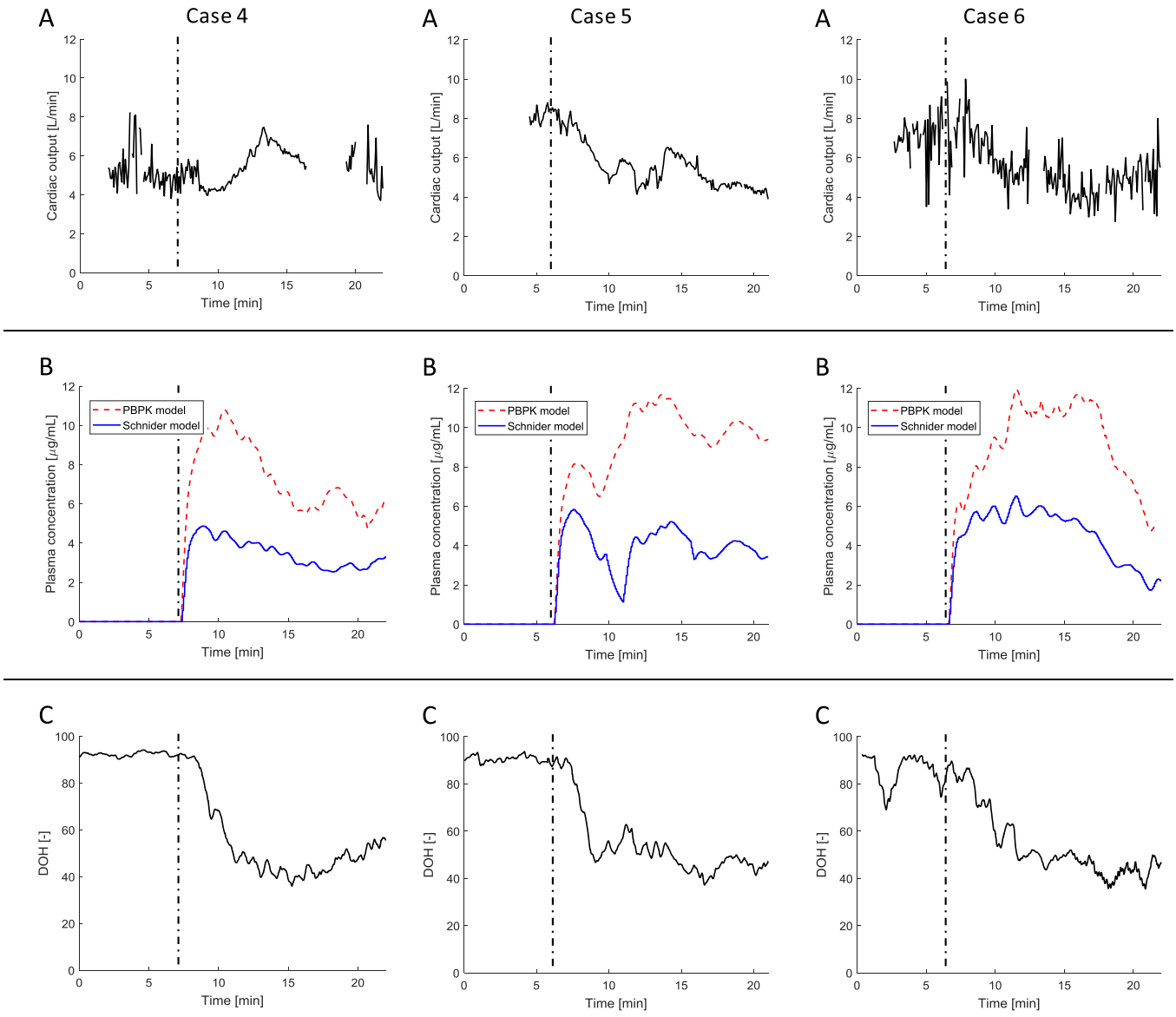

Fig. 3. Panel A shows the CO trends of the individual patients (cases 4, 5, and 6). Panel B shows the comparison between the plasma concentration dynamics predicted by our PBPK model (red dashed line) and Schnider model (blue continuous line). Panel C shows corresponding trends of the WAV_{CNS} index as DoH measure. The black dashed-dotted vertical line marks the start of propofol infusion. (For interpretation of the references to color in this figure legend, the reader is referred to the web version of this article.)

in Fig. 4 shows the effect-site concentration dynamics obtained via the two different modeling strategies to better explain such considerations. For the sake of completeness, Appendix A reports the comparison of the PBPK-PD and three-compartment PK-PD models with DoH data for the whole set of six representative cases whose predicted pharmacokinetics and DoH data were shown in Section 4.1.

4.3. In silico *evaluation of the effect of CO on DoH*

Three different trends of CO have been used as input to the PK simulation of case 1, to evaluate the effect of different CO drops on the pharmacokinetics. The PD model identified in Section 4.2 is now used to simulate the effect of the three CO trends on the DoH. The experimental data for this patient showed a 70% drop in CO (15 min following the start of induction of anesthesia), as shown in Fig. 5, where the CO trend is smoothed using a moving average for a better visualization and comparison. Fig. 5 shows the impact of different magnitude of CO changes on plasma PK and DoH prediction. Panel A shows three different CO trends leading to (i) 70% (continuous black line), (ii) 50% (dashed black line), and (iii) 35% drops (dashed-dotted lines). Panels B and C show the corresponding predicted plasma concentration (in red) and DoH (in blue) dynamics, respectively. A 35% drop in CO produces a minimum predicted DoH value of 37, whereas additional CO decreases to 50% and 70% result in significant overshoots to 27 and 21, respectively.

The difference between a drop of 35% and 70% leads to a 31% difference in the area under the curve (AUC, *i.e.* the area under the plasma drug concentration-time curve, reflecting the actual body exposure to drug) (see Table 6). These changes can be clinically relevant especially in “at-risk” patients. In fact, studies show that intraoperative burst suppression is associated with increased mortality [44-46] and post-operative delirium [46, 47], with impact on lengths of stay in the intensive care unit and hospital costs.

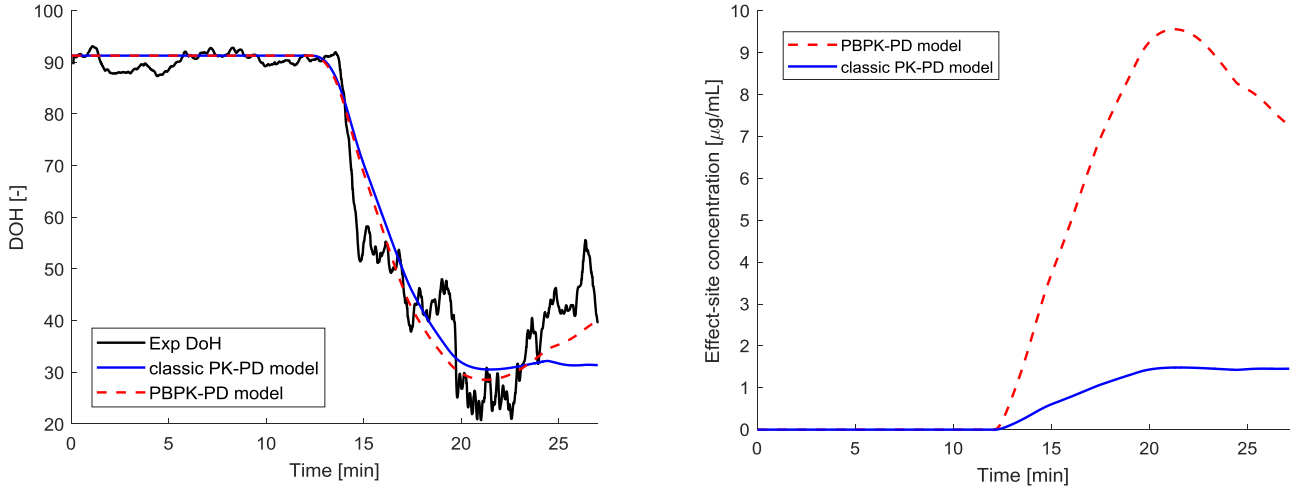

Fig. 4. Results of the PD model identification with DoH data of case 1 (black continuous line). Comparison of the DoH (left panel) and the effect-site concentration (right panel) dynamics obtained via PBPK-PD model (red dashed line) and the three-compartment PK-PD model (blue continuous line). (For interpretation of the references to color in this figure legend, the reader is referred to the web version of this article.)

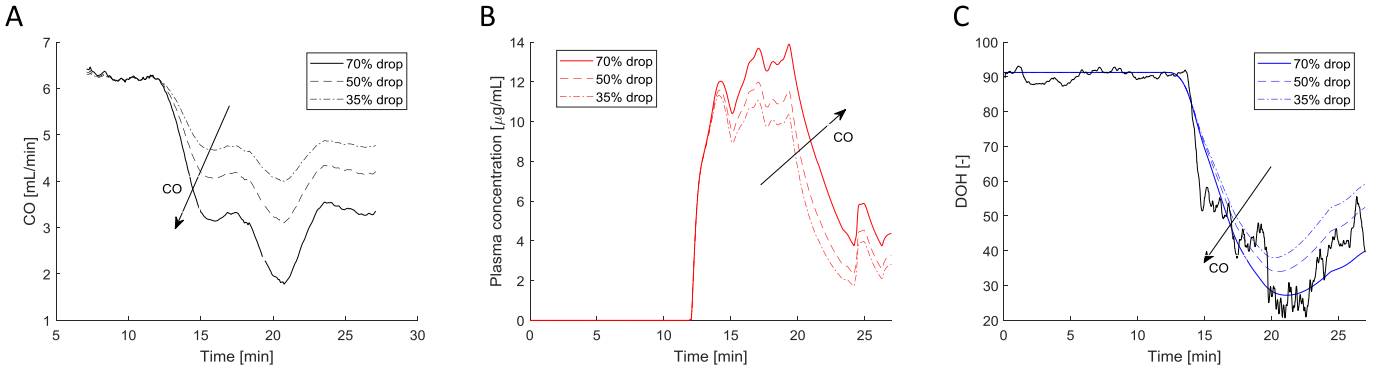

Fig. 5. Panel A shows different trends (black line) of CO corresponding to (i) 70% drop (as in case 1, continuous line), (ii) 50% drop (dashed line), (iii) 35% drop (dotted-dashed line). Panel B shows corresponding plasma PBPK predictions (red) and Panel C DoH predictions (blue) (simulated via combined Hill function). Experimental data (black continuous line) in Panel C shows DoH trend for case 1. The black arrow points in the direction of CO decrease. (For interpretation of the references to color in this figure legend, the reader is referred to the web version of this article.)

Table 6
AUC and minimum DoH values corresponding to the three simulated CO drop extents.

	AUC [(min mg)/mL]	DoH_{min} [-]
35% drop	110.47	34
50% drop	133.30	27
70% drop	145.58	21

5. Discussion and study limitations

Anesthesia is a complex multivariable process and some underlying mechanisms are to date not fully elucidated. The use of more mechanistic, detailed PK models, based on the anatomy and physiology of the human body, allows us to go beyond the goals of pharmacokinetic description and data fitting, typical of the empirically-based three-compartment models. Interestingly, we found PBPK simulations predicted high plasma peaks reflective of excessively deep anesthesia, as a result of marked decreases in CO. The integration of clinical data with PBPK simulations can represent a starting point for:

(i) Hypotheses-making on how the cardiovascular changes affect the pharmacokinetics of anesthetic and analgesic drugs not only in plasma but also in the effect-site, and the resulting depth DoH;

(ii) Design of experimental studies with the purpose of verifying and supplementing current knowledge on how factors such as CO variation affect propofol brain uptake and transfer across the blood-brain barrier.

Whereas we used clinical data to identify the parameters of a Hill-form equation to simulate DoH, the PBPK model was defined based on data from the literature [25] (see Table 2). No PK data were available from West et al. [20]. This means that the PK results need to be confirmed with additional experimental data, and specific studies are required to better define and understand the contributions of overdosing and changes in CO on excessively deep anesthesia levels.

As previously mentioned, although it is known that changes in CO and MAP affect drugs pharmacokinetics, three-compartment PK models commonly used to analyze the pharmacokinetics of IV analgesic and anesthetic drugs are not appropriate to investigate these effects. In fact, their parameters are either fixed or only include patient demographics as covariates. As far as we know, similar points have been discussed by only two other works: Reekers [48] and Upton and Ludbrook [19], who both employed a recirculatory model. In case of Reekers [48], however, the model parameters do not seem to include any covariates (*e.g.*, body mass, height, and gender). In addition, all of those parameters are identified with pharmacokinetic data, except for the venous lag time and CO. The model from Reekers [48] aims to describe propofol pharmacokinet-

ics, rather than predicting and simulating virtual patients for investigation of the effects of the cardiovascular changes. In [19], an interesting PBPK model is presented, in which blood flows are used to determine parameters of the final pharmacokinetic outcome. The methodology employed in our study attempts to improve the work from Upton and Ludbrook [19] in at least two aspects. Firstly, the compartment volumes are also anatomically-based and estimated depending on the patients' characteristics. This has a direct effect on the physiological feature of the model and makes it more flexible and individualized. Secondly, assumptions on propofol metabolism and elimination pathways are based on the literature where these pathways are hepatic, renal, and tissue-based (probably gastrointestinal) [49, 50].

6. Conclusions

This study has provided quantification of the response of high-risk patients to closed-loop induction in terms of CO, MAP, and HR. Since hemodynamics is an essential contributor to these patients' safety, evaluation of such effects is extremely valuable, especially compared to the available data on hemodynamic effects of propofol induction in the literature.

The second part of the study covered the impact of cardiovascular changes on propofol pharmacokinetics and pharmacodynamics, using a PBPK-PD modeling approach. We showed that a significant decrease in CO can lead to predicted plasma levels that cannot be calculated by three-compartment PK models. These traditional PK models, which are in routine daily use in anesthesia, may result in an amplified response in high-risk patients. This conclusion is supported by an improved prediction in the fitting of PD data with a PBPK model rather than the Schnider PK model.

Thus, the integration of CO data with PBPK simulations sheds light on the DoH outcome and offers interpretations of the inter-patient variability of the response to propofol. Although a limited number of patients were analyzed, and no pharmacokinetic data were available, these results show that PBPK- PD simulations can be employed to study and quantify the effect of the changes in CO on the DoH levels, as a rigorous investigation tool with potential applications ranging from training and education to improvement of the clinical practice through a better understanding of the impact of the hemodynamic changes on the patients DoH.

Our results may suggest that the use of PBPK model-based closed-loop systems would allow accounting for hemodynamic effects during closed-loop control of anesthesia. Adjusting the infusion rates also based on the hemodynamic data may limit the chance of overdosing in critical patients. CO is not always monitored in every patient, thus making this feature of PBPK modeling less useful. However, the awareness of the importance of flow monitoring in high-risk populations is increasing [51] and minimally invasive monitoring techniques are under development. In cases when CO is not directly monitored, correlations that infer CO from noninvasive data on either BP or perfusion can be developed and implemented.

Declaration of Competing Interest

The authors declare that they do not have any conflicts of interest.

Appendix A

Fig. A1.

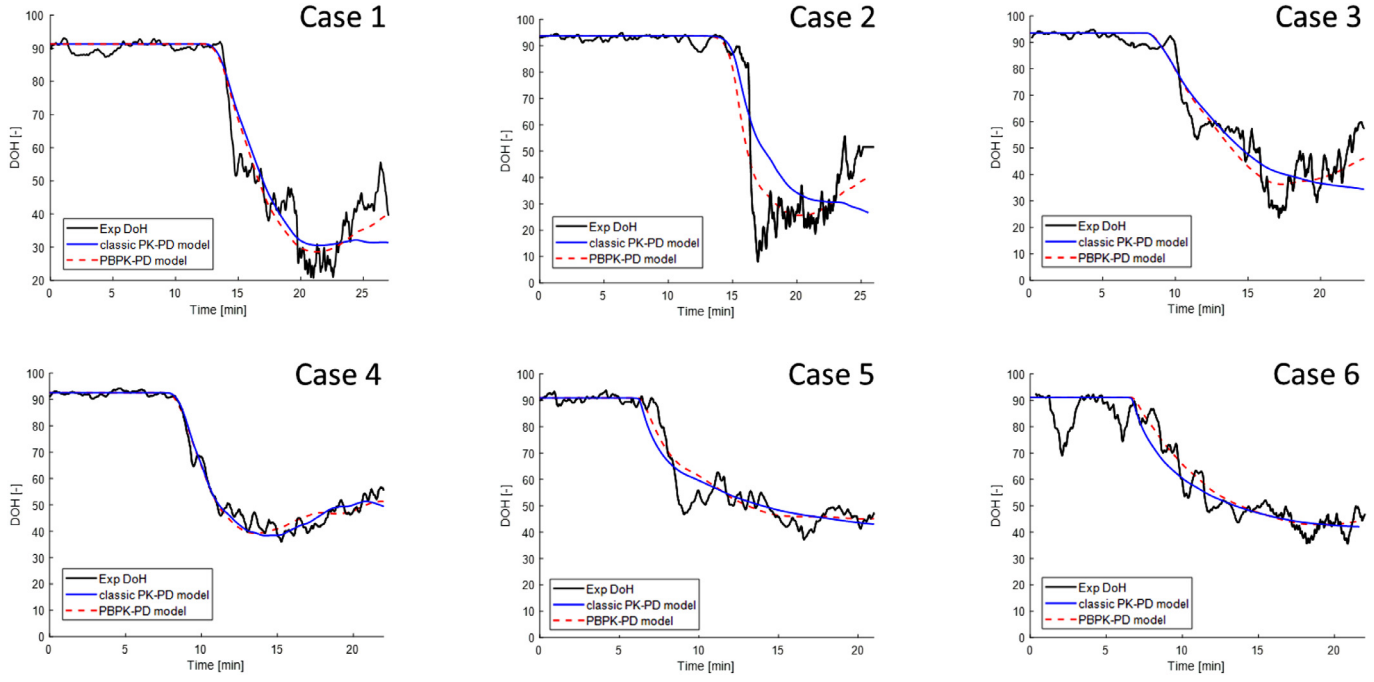

Fig. A.1. Results of the PD model identification with DoH data (black continuous line) for the considered six representative cases. Comparison of the PBPK-PD (red dashed line) and three-compartment PK-PD (blue continuous line) models. Cases 1, 2, and 3 feature $\%\Delta CO_{max} > 45$ coinciding with DoH overshoots. Cases 4, 5, and 6 feature more gradual and limited CO drops and acceptable DoH levels. (For interpretation of the references to color in this figure legend, the reader is referred to the web version of this article.)

References

[1] T. Kazama, K. Ikeda, K. Morita, M. Kikura, M. Doi, T. Ikeda, T. Kurita, Y. Nakajima, Comparison of the effect-site k(eO)s of propofol for blood pressure and EEG bispectral index in elderly and younger patients, Anesthesiology 90 (1999) 1517–1527.

[2] D.L. Reich, S. Hossain, M. Krol, B. Baez, P. Patel, A. Bernstein, C.A. Bodian, Predictors of hypotension after induction of general anesthesia, Anesth. Analg. 101 (2005) 622–628.

[3] M.J. Devinney, R.D. Sanders, R.M. Bauer, Climbing the delirium mountain: is alpine anaesthesia the perioperative cause? BJA 115 (2015) 342–344.

[4] L.F. Laso, A. López-Picado, E.O. de La Fuente, A.M. Murua, C. Sánchez-Castro, L.P. Ruilope, C. Valero-Martínez, Manual vs. target-controlled infusion induction with propofol: an observational study, Colomb. J. Anesthesiol. 44 (2016) 272–277.

[5] J.-L. Vincent, D. Fagnoul, Do we need to monitor cardiac output during major surgery? Anesthesiology 117 (2012) 1151–1152.

[6] R. Larsen, J. Rathgeber, A. Bagdahn, H. Lange, H. Rieke, Effects of propofol on cardiovascular dynamics and coronary blood flow in geriatric patients. A comparison with etomidate, Anaesthesia 43 (Suppl) (1988) 25–31.

[7] S. Bendel, E. Ruokonen, P. Polonen, A. Uusaro, Propofol causes more hypotension than etomidate in patients with severe aortic stenosis: a double-blind, randomized study comparing propofol and etomidate, Acta Anaesth. Scand. 51 (2007) 284–289.

[8] I. Potočnik, V.N. Janković, T. Štupnik, B. Kremžar, Haemodynamic changes after induction of anaesthesia with sevoflurane vs. propofol, Signa Vitae 6 (2011) 52–57.

[9] M.A. Claeys, E. Gepts, F. Camu, Haemodynamic changes during anaesthesia induced and maintained with propofol, Br. J. Anaesth. 60 (1988) 3–9.

[10] J.E. Fairfield, A. Dritsas, R.J. Beale, Haemodynamic effects of propofol: induction with 2.5 mg kg^{-1}, Br. J. Anaesth. 67 (1991) 618–620.

[11] A. Steib, G. Freys, J.P. Beller, U. Curzola, J.C. Otteni, Propofol in elderly high risk patients. A comparison of haemodynamic effects with thiopentone during induction of anaesthesia, Anaesthesia 43 (1988) 111–114.

[12] M. Janda, O. Simanski, J. Bajorat, B. Pohl, G.F. Noeldge-Schomburg, R. Hofmockel, Clinical evaluation of a simultaneous closed-loop anaesthesia control system for depth of anaesthesia and neuromuscular blockade*, Anaesthesia 66 (2011) 1112–1120.

[13] F.N. Nogueira, T. Mendonça, P. Rocha, Controlling the depth of anesthesia by a novel positive control strategy, Comput. Methods Programs Biomed. 114 (2014) e87–e97.

[14] F. Padula, C. Ionescu, N. Latronico, M. Paltenghi, A. Visioli, G. Vivacqua, Optimized PID control of depth of hypnosis in anesthesia, Comput. Methods Programs Biomed. 144 (2017) 21–35.

[15] R.N. Upton, G.L. Ludbrook, C. Grant, A.M. Martinez, Cardiac output is a determinant of the initial concentrations of propofol after short-infusion administration, Anesth. Analg. 89 (1999) 545–552.

[16] Y.U. Adachi, K. Watanabe, H. Higuchi, T. Satoh, The determinants of propofol induction of anesthesia dose, Anesth. Analg.Anesth. Analg. 92 (2001) 656–661.

[17] S.M. Brodie, M. Gorges, J.M. Ansermino, G.A. Dumont, R.N. Merchant, Closed-loop control of total intravenous anesthesia during significant intraoperative blood loss: a case report, A&A Case Rep. 9 (2017) 239–243.

[18] T. Kurita, K. Morita, T. Kazama, S. Sato, Influence of cardiac output on plasma propofol concentrations during constant infusion in swine, Anesthesiology 96 (2002) 1498–1503.

[19] R.N. Upton, G. Ludbrook, A physiologically based, recirculatory model of the kinetics and dynamics of propofol in man, Anesthesiology 103 (2005) 344–352.

[20] N. West, K. van Heusden, M. Gorges, S. Brodie, A. Rollinson, C.L. Petersen, G.A. Dumont, J.M. Ansermino, R.N. Merchant, Design and evaluation of a closed-loop anesthesia system with robust control and safety system, Anesth. Analg. 127 (2018) 883–894.

[21] A. Savoca, D. Manca, A physiologically-based approach to model-predictive control of anesthesia and analgesia, Biomed. Signal Process. Control 53 (2019) 101553.

[22] R.A. Abbiati, A. Savoca, D. Manca, Chapter 2 - An engineering oriented approach to physiologically based pharmacokinetic and pharmacodynamic modeling, in: D. Manca (Ed.), Computer Aided Chemical Engineering, Elsevier, 2018, pp. 37–63.

[23] F. Stader, M. Siccardi, M. Battegay, H. Kinvig, M.A. Penny, C. Marzolini, Repository describing an aging population to inform physiologically based pharmacokinetic models considering anatomical, physiological, and biological age-dependent changes, Clin. Pharmacokinet. 58 (2019) 483–501.

[24] J.X. Mazoit, K. Samii, Binding of propofol to blood components: implications for pharmacokinetics and for pharmacodynamics, Br. J. Clin. Pharmacol. 47 (1999) 35–42.

[25] T.W. Schnider, C.F. Minto, P.L. Gambus, C. Andresen, D.B. Goodale, S.L. Shafer, E.J. Youngs, The influence of method of administration and covariates on the pharmacokinetics of propofol in adult volunteers, Anesthesiology 88 (1998) 1170–1182.

[26] F. Servin, R. Farinotti, J.P. Haberer, J.M. Desmonts, Propofol infusion for maintenance of anesthesia in morbidly obese patients receiving nitrous oxide. A clinical and pharmacokinetic study, Anesthesiology 78 (1993) 657–665.

[27] J. Dyck, S.L. Shafer, Effects of age on propofol pharmacokinetics, Semin. Anesth. 11 (1992) 2–4.

[28] P. Smuszkiewicz, P. Wiczling, K. Przybylowski, A. Borsuk, I. Trojanowska, M. Paterska, J. Matysiak, Z. Kokot, E. Grzeskowiak, A. Bienert, The pharmacokinetics of propofol in ICU patients undergoing long-term sedation, Biopharm. Drug Dispos. 37 (2016) 456–466.

[29] E. Gepts, F. Camu, I.D. Cockshott, E.J. Douglas, Disposition of propofol administered as constant rate intravenous infusions in humans, Anesth. Analg. 66 (1987) 1256–1263.

[30] J. Valentin, Basic anatomical and physiological data for use in radiological protection: reference values: ICRP Publication 89, Ann. ICRP 32 (2002) 1–277.

[31] M. Hara, K. Masui, D.J. Eleveld, M. Struys, O. Uchida, Predictive performance of eleven pharmacokinetic models for propofol infusion in children for long-duration anaesthesia, Br. J. Anaesth. 118 (2017) 415–423.

[32] D.J. Eleveld, P. Colin, A.R. Absalom, M. Struys, Pharmacokinetic-pharmacodynamic model for propofol for broad application in anaesthesia and sedation, Br. J. Anaesth. 120 (2018) 942–959.

[33] R. Singh, M. Choudhury, P.M. Kapoor, U. Kiran, A randomized trial of anesthetic induction agents in patients with coronary artery disease and left ventricular dysfunction, Ann. Cardiac Anaesth. 13 (2010) 217–223.

[34] J.J. Vos, M. Poterman, L.N. Hannivoort, V.W. Renardel De Lavalette, M.M. Struys, T.W. Scheeren, A.F. Kalmar, Hemodynamics and tissue oxygenation during balanced anesthesia with a high antinociceptive contribution: an observational study, Perioper. Med. 3 (2014) 9.

[35] M.J. Coppens, D.J. Eleveld, J.H. Proost, L.A. Marks, J.F. Van Bocxlaer, H. Vereecke, A.R. Absalom, M.M. Struys, An evaluation of using population pharmacokinetic models to estimate pharmacodynamic parameters for propofol and bispectral index in children, Anesthesiology 115 (2011) 83–93.

[36] K. Masui, R.N. Upton, A.G. Doufas, J.F. Coetzee, T. Kazama, E.P. Mortier, M.M. Struys, The performance of compartmental and physiologically based recirculatory pharmacokinetic models for propofol: a comparison using bolus, continuous, and target-controlled infusion data, Anesth. Analg. 111 (2010) 368–379.

[37] L.I. Cortinez, What is the ke0 and what does it tell me about propofol? Anaesthesia 69 (2014) 399–402.

[38] M.M. Struys, M.J. Coppens, N. De Neve, E.P. Mortier, A.G. Doufas, J.F. Van Bocxlaer, S.L. Shafer, Influence of administration rate on propofol plasma-effect site equilibration, Anesthesiology 107 (2007) 386–396.

[39] T. Kirkpatrick, I.D. Cockshott, E.J. Douglas, W.S. Nimmo, Pharmacokinetics of propofol (diprivan) in elderly patients, Br. J. Anaesth. 60 (1988) 146–150.

[40] J. Vuyk, C.J. Oostwouder, A.A. Vletter, A.G.L. Burm, J.G. Bovill, Gender differences in the pharmacokinetics of propofol in elderly patients during and after continuous infusion, BJA 86 (2001) 183–188.

[41] L.I. Cortinez, N. De la Fuente, D.J. Eleveld, A. Oliveros, F. Crovari, P. Sepulveda, M. Ibacache, S. Solari, Performance of propofol target-controlled infusion models in the obese: pharmacokinetic and pharmacodynamic analysis, Anesth. Analg. 119 (2014) 302–310.

[42] J.C. Drummond, Blood pressure and the brain: how low can you go? Anesth. Analg. 128 (2019) 759–771.

[43] A.A. Dahaba, J.X. Xue, Y. Hua, Q.H. Liu, G.X. Xu, Y.M. Liu, X.F. Meng, G.G. Zhao, P.H. Rehak, H. Metzler, The utility of using the bispectral index-vista for detecting cross-clamping decline in cerebral blood flow velocity, Neurosurgery 67 (2010) ons102-107; discussion ons107.

[44] P.L. Watson, A.K. Shintani, R. Tyson, P.P. Pandharipande, B.T. Pun, E.W. Ely, Presence of electroencephalogram burst suppression in sedated, critically ill patients is associated with increased mortality, Critic. Care Med. 36 (2008) 3171.

[45] M.D. Kertai, N. Pal, B.J. Palanca, N. Lin, S.A. Searleman, L. Zhang, B.A. Burnside, K.J. Finkel, M.S. Avidan, Association of perioperative risk factors and cumulative duration of low bispectral index with intermediate-term mortality after cardiac surgery in the B-Unaware Trial, Anesthesiology 112 (2010) 1116–1127.

[46] J.M. Andresen, T.D. Girard, P.P. Pandharipande, M.A. Davidson, E.W. Ely, P.L. Watson, Burst suppression on processed electroencephalography as a predictor of post-coma delirium in mechanically ventilated ICU patients, Critic. Care Med. 42 (2014) 2244.

[47] M. Soehle, A. Dittmann, R.K. Ellerkmann, G. Baumgarten, C. Putensen, U. Guenther, Intraoperative burst suppression is associated with postoperative delirium following cardiac surgery: a prospective, observational study, BMC Anesth. 15 (2015) 61.

[48] M. Reekers, Recirculatory Modeling in Man Using Indocyanine Green, 2012.

[49] H. Hiraoka, K. Yamamoto, S. Miyoshi, T. Morita, K. Nakamura, Y. Kadoi, F. Kunimoto, R. Horiuchi, Kidneys contribute to the extrahepatic clearance of propofol in humans, but not lungs and brain, Br. J. Clin. Pharmacol. 60 (2005) 176–182.

[50] P.A. Gray, G.R. Park, I.D. Cockshott, E.J. Douglas, B. Shuker, P.J. Simons, Propofol metabolism in man during the anhepatic and reperfusion phases of liver transplantation, Xenobiotica 22 (1992) 105–114.

[51] D. Green, H. Bidd, H. Rashid, Multimodal intraoperative monitoring: an observational case series in high risk patients undergoing major peripheral vascular surgery, Int. J. Surg. 12 (2014) 231–236.